INSTITUTE OF PHYSICS PUBLISHING PHYSICS IN MEDICINE AND BIOLOGY

Phys. Med. Biol. **48** (2003) 2169–2181 PII: S0031-9155(03)60044-8

Effect of spurt duration on the heat transfer dynamics during cryogen spray cooling

Guillermo Aguilar[1,2], **Guo-Xiang Wang**[3] **and J Stuart Nelson**[1,2]

[1] Department of Biomedical Engineering, University of California, Irvine, CA 92697, USA
[2] Beckman Laser Institute, University of California, 1002 Health Sciences Road East, Irvine, CA 92612-1475, USA
[3] Department of Mechanical Engineering, University of Akron, OH 44325, USA

E-mail: gaguilar@bli.uci.edu.

Received 26 February 2003, in final form 21 May 2003
Published 1 July 2003
Online at stacks.iop.org/PMB/48/2169

Abstract

Although cryogen spray cooling (CSC) is used to minimize the risk of epidermal damage during laser dermatologic surgery, optimization of the current cooling approach is needed to permit the safe use of higher light doses, which should improve the therapeutic outcome in many patients. The objective of this study was to measure the effect of spurt duration (Δt) on the heat transfer dynamics during CSC using a model skin phantom. A fast-response temperature sensor was constructed to record the changes in surface temperature during CSC. Temperature measurements as a function of Δt at two nozzle-to-skin distances ($z = 50$ and 20 mm) were performed. The average surface heat fluxes (q) and heat transfer coefficients (h) for each Δt were computed using an inverse heat conduction problem algorithm. It was observed that q undergoes a marked dynamic variation during the entire Δt, with a maximum heat flux (q_c) occurring early in the spurt (5–15 ms), followed by a quick decrease. The estimated q_c vary from 450 to 600 kW m^{-2}, corresponding to h maxima of 10 and 17–22 kW m^{-2} K^{-1} for $z = 50$ and 20 mm, respectively. For $z = 50$ mm, spurts longer than 40 ms do not increase the total heat removal (Q) within the first 200 ms. However, for $z = 20$ mm, Δt longer than 100 ms are required to achieve the same Q. It is shown that the heat transfer dynamics and the time it takes to reach q_c during CSC can be understood through classic boiling theory as a transition from transient to nucleate boiling. Based on the results of this model skin phantom, it is shown that spurts longer than 40 ms have a negligible impact on both q and Q within clinically relevant cooling times (10–100 ms).

(Some figures in this article are in colour only in the electronic version)

1. Introduction

Cryogen spray cooling (CSC) is used in conjunction with various dermatologic laser surgeries (Nelson *et al* 1995, 2000, Waldorf *et al* 1997, Chang *et al* 1998, Kelly *et al* 1999, Verkruysse *et al* 2000). The purpose of CSC is to cool selectively the epidermis to prevent excessive epidermal heating after laser irradiation, while deeper targeted chromophores are thermally photocoagulated. During CSC, the skin surface is sprayed with tetrafluoroethane (R-134a) for a short period of time (10–100 ms). R-134a in liquid state is released from a pressurized container through a valve–nozzle system and atomized into small droplets (3–20 μm) (Aguilar *et al* 2000, 2001b). Since R-134a is volatile at atmospheric conditions, droplets evaporate while moving towards the skin surface at high speed (10–60 m s^{-1}) (Aguilar *et al* 2000). As a result, the low liquid temperature (-26 to -60 °C) (Aguilar *et al* 2000, 2001b) of the impinging cryogen droplets can effectively cool the skin surface.

The main parameter that characterizes spray cooling is the heat flux (q) through the skin surface. However, some researchers employ the heat transfer coefficient, h, instead of q to quantify heat transfer during CSC (Majaron *et al* 2001, Pfefer *et al* 2000, Aguilar *et al* 2002). The two parameters are related through Newton's cooling law:

$$q = hA(T - T_c) \tag{1}$$

where A represents the sprayed surface area, T the surface temperature and T_c an average temperature of the liquid cryogen in contact with skin. A drawback of using h to quantify the heat transfer during CSC is that its value is determined indirectly using equation (1) and, for that purpose, a constant T_c must be defined. Since the magnitude of T_c is an arbitrary choice, different values of h may actually represent the same q. On the other hand, q is unequivocally determined through direct experimental measurements.

Studies to quantify h or q during CSC were carried out by Anvari *et al* (1998), who measured the change in skin surface temperature using infrared thermometry. An average h value of 40 kW m^{-2} K^{-1} was estimated using $T_c = -7$ °C for spurt durations (Δt) ranging from 5 to 80 ms with a nozzle-to-skin distance (z) of 20 mm. Torres *et al* (2001) used an epoxy block with 30 μm thermocouples embedded at different depths ranging from 20 to 400 μm and an inverse heat conduction problem (IHCP) algorithm to obtain a rather low value for h ($\sim$2.4 kW m^{-2} K^{-1}) based on a constant $T_c \approx -44$ °C. Recent studies using a refined IHCP algorithm (Tunnell *et al* 2002), as well as other experimental techniques based on constant q (Aguilar *et al* 2001c) or lumped capacitance (Svaasand *et al* 2003, Aguilar *et al* 2001a) principles, showed that for similar CSC conditions, h varies between the two values previously reported (Anvari *et al* 1998, Torres *et al* 2001).

In addition to the selection of T_c, several other factors may contribute to the wide range of values reported for h. The most important factor is the response time of the temperature sensors. For example, the thermal relaxation time of large silver disc sensors used in previous studies (Svaasand *et al* 2003, Aguilar *et al* 2001a) was of the order of 100 ms. Therefore, the values of h previously published only provide an average estimate for 100 ms spurts. However, since Δt is of the order of tens of milliseconds, fast-response temperature sensors should be employed to measure rapid changes in the surface temperature during CSC.

It is clear, however, that to cool selectively the epidermis prior to laser irradiation, cryogen spurts should produce high q at the skin surface and that two key parameters must be optimized: Δt and z. In clinical practice, it is possible to select different Δt, typically 10–100 ms. However, z is always fixed by the handpiece unique to each commercial device. Because cryogen droplets evaporate during flight, z should also be optimized to achieve higher q.

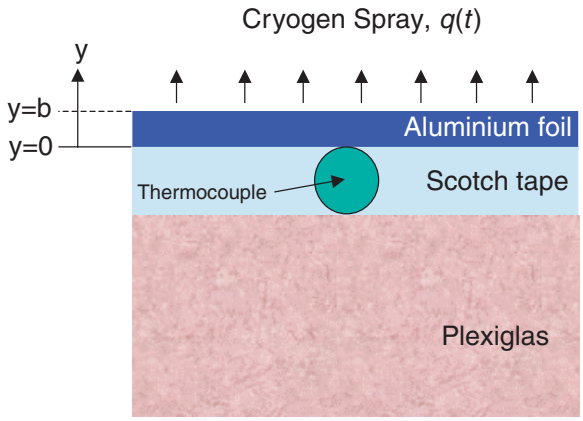

Figure 1. Model of one-dimensional inverse heat transfer (not to scale). Note that the measured temperature data are closer to the point of best thermal contact, i.e., at the interface $y = 0$. Aluminium foil and Scotch tape thicknesses are 20 and 50 μm, respectively.

A fast temperature sensor was recently introduced (Aguilar *et al* 2003) with a response time of the order of a few milliseconds, which can measure rapid changes in the skin surface temperature during CSC. Using this sensor, it was found that there are two different CSC regimes, which depend on z (Aguilar *et al* 2003). When z is greater than 25 mm, the spray is more finely atomized before reaching the surface and, therefore, a thicker cryogen layer forms on the skin surface. The presence of this layer prevents the skin surface from cooling beyond a certain minimum which impairs q. In contrast, when z is less than 25 mm, larger and faster droplets impinge on the skin more forcefully, leading to a thinner cryogen layer that quickly evaporates. As a result, lower minimum temperatures are achieved and, consequently, q is enhanced.

In this paper, the fast temperature sensor is used along with a refined IHCP algorithm to determine experimentally q and h as functions of time. The focus is only on the effect of spurt duration (Δt) on the cooling dynamics for two spray distances, $z = 50$ and 20 mm.

2. Experimental methods and procedures

2.1. Temperature measurement sensor

The temperature sensor consists of a miniature type-K thermocouple ($\sim$50 μm bead diameter) placed underneath a thin (20 μm) layer of aluminium foil (15 mm $\times$ 10 mm) (figure 1). The aluminium foil is positioned on top of a 12.5 mm square bar of polymethyl methacrylate resin (Plexiglas®). Small strips of 50 μm thick cellulose tape (Scotch tape®) are placed between the aluminium foil and the Plexiglas® bar, forming a square box around the thermocouple bead and providing thermal insulation and mechanical support. Thermal paste is applied around the bead to ensure good thermal contact. The purpose of this sensor is to provide a skin-like thermal substrate, so that the total heat removal, Q, and surface heat flux, q, are of the same order of magnitude as those expected for human skin. The small metallic foil coupled with a miniature temperature sensor provides 'real-time' surface temperature measurements. Since Plexiglas® and Scotch tape® are thermal insulators, the temperature measurement at the interface ($y = 0$) is likely to be very close to that of the aluminium foil. Published thermal

Table 1. Thermal properties and thicknesses of layers used in the temperature measurement sensor. Human epidermal skin properties are provided for reference.

Properties	Al foil	Scotch tape®	Plexiglas®	Epidermis
Thickness (mm)	0.020	0.050	19	–
k (W m^{-1} K^{-1})	205	0.19–0.25	0.19–0.24	0.21
ρ (kg m^{-3})	2710	1160–1400	1150–1190	1200
c (J kg^{-1} K^{-1})	896	1400	1300–1500	3600
α_{avg} (m^2 s^{-1})	844×10^{-7}	1.22×10^{-7}	1.31×10^{-7}	0.486×10^{-7}

properties of the materials used to build the sensor are shown in table 1. Thermal properties of epidermal human skin (Duck 1990) are also given for reference.

All thermocouple measurements are acquired at 4 kHz and converted to temperature data using an A/D converter board and dedicated software (InstruNet™, Omega Engineering, Stamford, CT). This acquisition rate is appropriate because the response time (τ) of the aluminium foil attached to the thermocouple sensor is less than 3 ms.

2.2. Cryogen delivery and nozzle

The cryogen utilized is 1,1,1,2-tetrafluoroethane, also known as R-134a, with boiling temperature $T_b \approx -26\ ^\circ$C at atmospheric pressure. Cryogen is kept in a container at saturation pressure (660 kPa at 25 °C), and delivered through a high-pressure hose to an electronically controlled fuel injector attached to a straight-tube nozzle. The nozzle is made of stainless steel with an inner diameter (d_N) and a length (l_N) of 0.7 mm and 63.6 mm, respectively. The nozzle is soldered to a custom-made copper coupling, which in turn fits tightly around the fuel injector. d_N is similar to that of commercial devices.

2.3. Mathematical model and inverse heat transfer algorithm

CSC can be simplified to a one-dimensional heat conduction problem if a uniform heat transfer over the sprayed surface (figure 1) is assumed. An IHCP algorithm is solved using the measured surface temperature as input. Many algorithms have been developed to solve such an inverse problem (Taler 1996, Beck *et al* 1985) and the sequential function specification method (SFSM) of Beck *et al* (1985) is employed here. SFSM estimates q as a piecewise constant function of time, sequentially solving for q at each time step. Tunnell *et al* (2002) provided a detailed discussion of this algorithm as applied to CSC.

Using the layered structure and the coordinate system given in figure 1, the SFSM solves a one-dimensional heat conduction problem given by the following equation:

$$\rho_j c_j \frac{\partial T_j}{\partial t} = k_j \frac{\partial^2 T_j}{\partial y^2} \tag{2}$$

where ρ is the density, c is the specific heat, k is the thermal conductivity and the subscript j is replaced by Al, ST or PG when equation (2) is applied to the aluminium foil, Scotch tape and Plexiglas® layers, respectively. The Plexiglas® can be treated as a semi-infinite thick body and, thus, only one boundary condition at the aluminium foil surface is needed:

$$-k_{Al} \left.\frac{\partial T_{Al}}{\partial y}\right|_{y=b} = q(t) \tag{3}$$

where b is the aluminium foil thickness and $q(t)$ is the surface heat flux that must be estimated.

SFSM assumes a functional form of the surface heat flux variation over any given discrete time period. The simplest function form is that $q(t)$ is a constant, which is used here. For an assumed constant heat flux (q_M^*) over time t_M to t_{M+1}, the governing equations (2) and (3) are solved for times t_M, $t_{M+1}, \ldots, t_{M+r-1}$, giving temperatures T_M^*, $T_{M+1}^*, \ldots, T_{M+r-1}^*$ at the corresponding time points at $y = 0$, where the temperature was measured during the experiment. One important feature of SFSM is that it uses the temperature information of future time steps, with r being the number of future time steps. More stable and physically sound results are obtained using multiple future steps, i.e., $r \geqslant 2$. In that case, the actual surface heat flux, q_M, can be calculated based on the assumed heat flux, q_M^* (Beck *et al* 1985, Tunnell *et al* 2002) as follows:

$$q_M = q_M^* + \frac{\sum_{i=1}^{r} (Y_{M+i-1} - T_{M+i-1}^*) Z_{i-1}}{\sum_{i=1}^{r} (Z_{i-1})^2} \tag{4}$$

where Z_i is the sensitivity coefficient, defined as

$$Z_i = \frac{\partial T_i}{\partial q_M} \qquad \text{at} \quad y = 0 \tag{5}$$

and Y_i is the measured temperature at time t_i. The sensitivity coefficient can be obtained by solving equation (2) with T_i replaced by Z_i but with a boundary condition

$$-k_{\mathrm{Al}} \left. \frac{\partial Z_i}{\partial y} \right|_{y=b} = 1 \tag{6}$$

under the same geometrical conditions.

2.4. Data smoothing and analysis

Raw data are affected by fluctuations, which may include random and ac noise. Thus, independent of the specific mathematical technique used in the IHCP, smoothing of the data is required for the numerical computation. For the data presented herein, a digital filter of least-squares fitting with orthogonal Gram polynomial of third degree (Taler 1996) over 11 equally spaced data points is used:

$$Y_M = Y(t_M) = \frac{1}{429} \begin{pmatrix} -36Y_{i-5} + 9Y_{i-4} + 44Y_{i-3} + 69Y_{i-2} + 84Y_{i-1} \\ +89Y_i + 84Y_{i+2} + 69Y_{i+2} + 44Y_{i+3} + 9Y_{i+4} - 36Y_{i+5} \end{pmatrix}. \tag{7}$$

Calculations indicate that such a digital filter is very effective in removing random noise.

3. Results

3.1. Dynamic heat transfer mechanism during CSC

Figure 2 shows the change in surface temperature for six Δt ranging from 10 to 100 ms for $z = 50$ mm. The surface temperature starts to slowly drop once the cryogen droplets impinge on the surface, but it decreases faster once the temperature drops below 10 °C. After the surface reaches the cryogen boiling temperature ($T_{\mathrm{b}} = -26$ °C, dashed line), the temperature decrease slows and finally reaches a minimum at −30 °C. If Δt is shorter than 20 ms, the surface temperature does not drop below T_{b} (e.g., for $\Delta t = 10$ ms, the minimum temperature is only −3 °C). For $\Delta t > 20$ ms, the surface temperature reaches a minimum of approximately −30 °C and slowly rises after spurt termination. It is apparent that the temperature profile is almost the same within the first 50 ms for any Δt longer than 20 ms. This suggests that a layer of liquid cryogen quickly builds up on the surface within 20 ms.

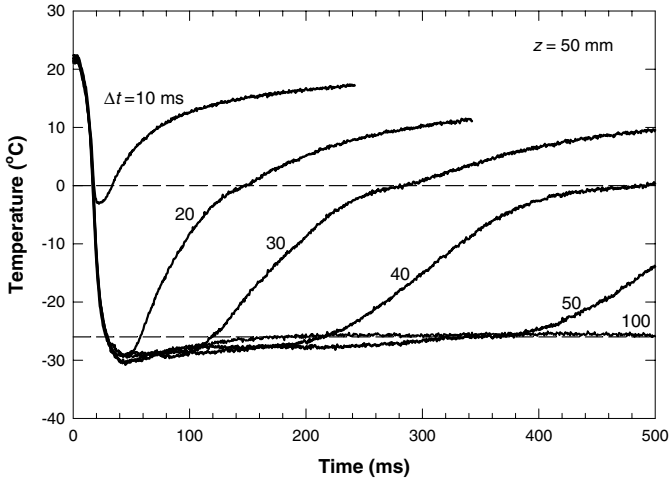

Figure 2. Measured temperature variation as a function of time for spurt durations: $\Delta t = 10$, 20, 30, 40, 50 and 100 ms; spray distance $z = 50$ mm.

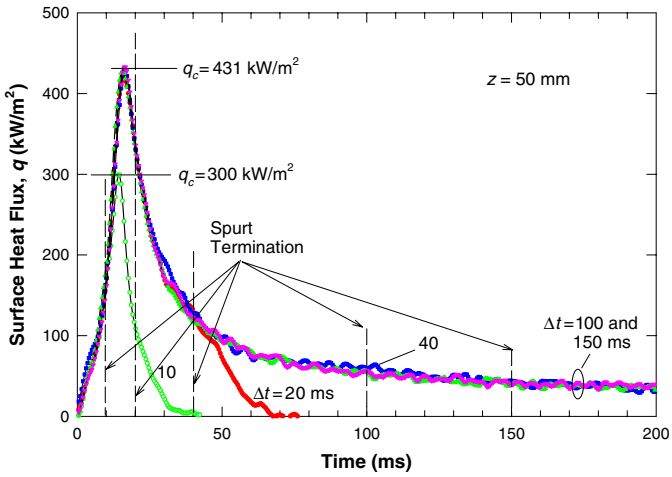

Figure 3. Estimated surface heat flux, q, as a function of time for five spurt durations: $\Delta t = 10$, 20, 40, 100 and 150 ms; spray distance $z = 50$ mm.

As the layer develops, the surface temperature drops quickly. Once the temperature has dropped below T_b, the surface temperature remains almost constant, until the liquid cryogen layer completely evaporates. Therefore, further prolonging Δt only increases the thickness of the liquid cryogen layer and will not further reduce the surface temperature.

3.2. Effect of Δt for $z = 50$ mm

Using these data, the surface heat flux (q) was estimated as a function of time, $q(t)$, by solving the IHCP algorithm. Figure 3 shows $q(t)$ for five Δt: 10, 20, 40, 100 and 150 ms. The dashed lines indicate spurt termination for each Δt. For all cases, $q(t)$ increases rapidly to a maximum value (q_c) and then drops quickly. Except for the two shortest spurts (10 and 20 ms), which

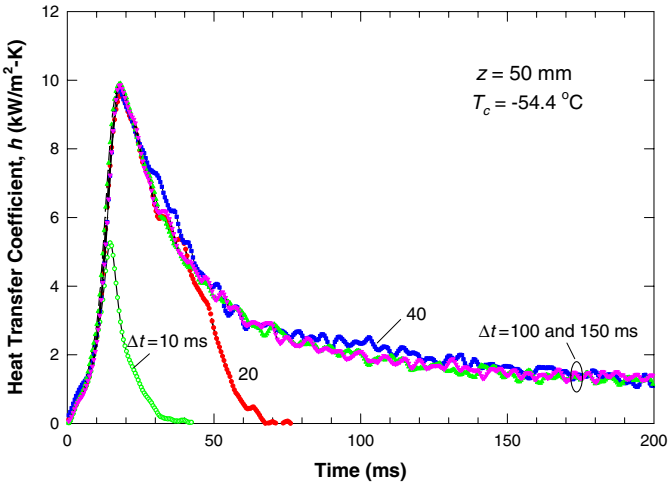

Figure 4. Estimated heat transfer coefficient, h, as a function of time for five spurt durations: $\Delta t = 10$, 20, 40, 100 and 150 ms; spray distance $z = 50$ mm.

result in short cooling times, all other Δt produce essentially the same $q(t)$ within the first 200 ms and, immediately after spurt termination, there is still a fairly high $q(t)$, which slowly declines thereafter. Extending Δt from 40 to 150 ms does not have any effect on $q(t)$ and an identical q_c value of 431 kW m^{-2} is reached for all Δt. This indicates that a very high rate of heat transfer occurs only in the first 40 ms of a spurt, when the surface temperature decreases rapidly. Once the surface temperature is below T_b, cooling is primarily dominated by heat conduction through the liquid layer, and the evaporation rate of cryogen from the surface. Further prolonging Δt only deposits more cryogen on the surface and, therefore, produces longer cooling times. This also implies that for $z = 50$ mm, the droplets' momentum is not sufficient to penetrate through the liquid layer and, thus, a longer Δt does not increase $q(t)$.

Figure 4 shows $h(t)$ corresponding to each of the $q(t)$ curves shown in figure 3. $h(t)$ is computed using equation (1) and a T_c value of -54.4 °C is used as the meaningful average cryogen layer temperature, which can be easily measured by placing a thermocouple within the spray cone (Aguilar *et al* 2001c). For $q(t)$, it is seen that for Δt longer than 40 ms, $h(t)$ is practically identical, where $h(t)$ increases to a maximum value of 9.8 kW m^{-2} K^{-1} within the first 16 ms and it drops exponentially to 1.1 kW m^{-2} K^{-1} at 200 ms. This is indicative of a long residence time for the liquid cryogen layer on the surface.

Finally, the total heat removal (Q) can also be determined numerically. Figure 5 shows the corresponding results for various Δt and $z = 50$ mm. It can be noted that Q is insensitive to Δt within the first 200 ms for all Δt longer than 40 ms.

3.3. Effect of Δt for $z = 20$ mm

Figure 6 shows the measured temperature variation as a function of time for various Δt ranging from 5 to 100 ms for $z = 20$ mm. Compared to figure 2, the surface temperature curves for $z = 20$ mm are very different and Δt shows a rather marked effect on surface cooling. As Δt becomes longer, the minimum surface temperature decreases further below that noted for $z = 50$ mm. However, the total cryogen residence time, defined as the time during which the surface temperature remains below T_b (Aguilar *et al* 2003), becomes much shorter, no more than 300 ms.

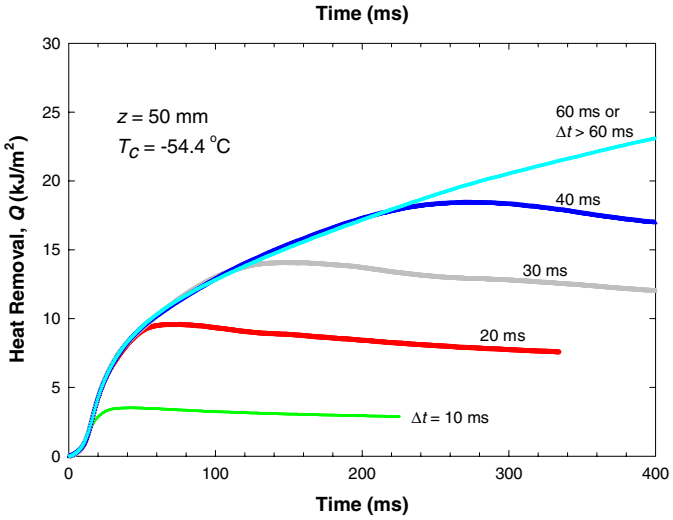

Figure 5. Estimated total heat removal per unit area, Q, as a function of time for five spurt durations: $\Delta t = 10$, 20, 30, 40 and 60 ms; spray distance $z = 50$ mm.

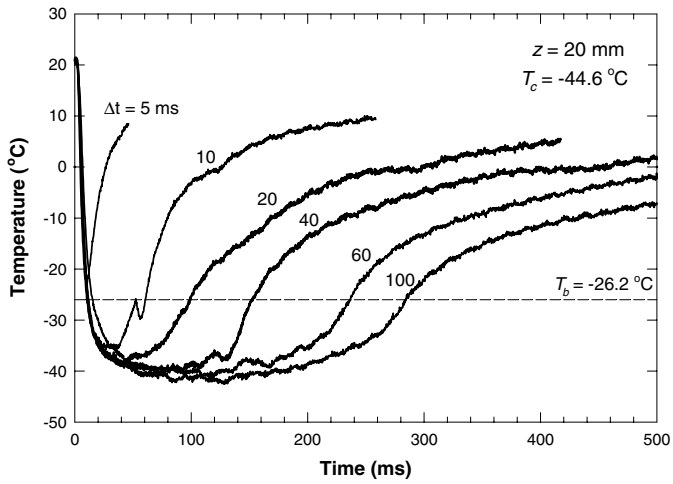

Figure 6. Measured temperature variation as a function of time for spurt durations: $\Delta t = 5$, 10, 20, 40, 60 and 100 ms; spray distance $z = 20$ mm.

The estimated $q(t)$ for four different Δt, 10, 30, 60 and 100 ms at $z = 20$ mm, are shown in figure 7. The heat transfer characteristics shown in figure 7 are qualitatively similar to those shown in figure 3 for $z = 50$ mm, with q_c occurring during the spurt and a slow decrease after spurt termination. For $z = 20$ mm, however, there is a significant increase in q_c from 550 to 620 kW m^{-2}, compared to 431 kW m^{-2} for $z = 50$ mm. In addition, the time needed to reach q_c is also shortened to 5 ms.

Figure 8 shows the corresponding heat transfer coefficient, $h(t)$ computed for the same Δt shown in figure 7 using the measured value of T_c (-44.6 °C) at $z = 20$ mm for this nozzle (Aguilar *et al* 2001c). The results reveal several interesting features of CSC for this z and a very different variation of $h(t)$ compared to that seen for $z = 50$ mm. For clarity,

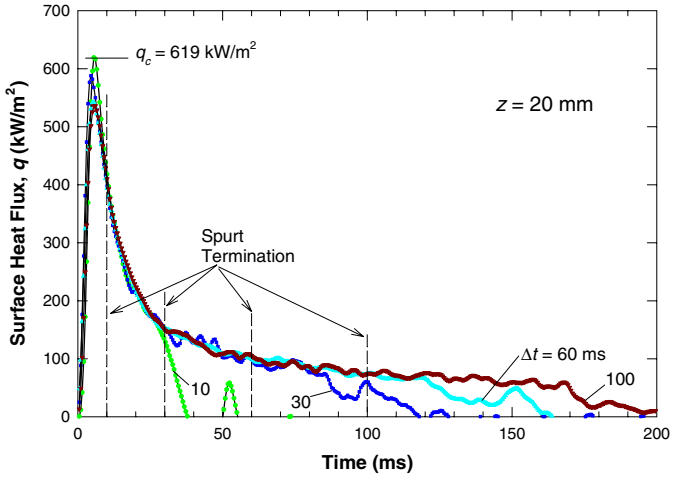

Figure 7. Estimated surface heat flux, q, as a function of time for spurt durations: $\Delta t = 10$, 30, 60 and 100 ms; spray distance $z = 20$ mm.

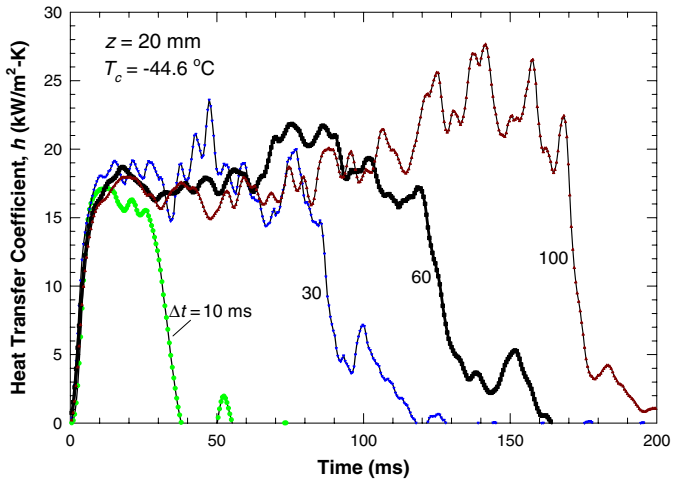

Figure 8. Estimated heat transfer coefficient, h, as a function of time for spurt durations: $\Delta t = 10$, 30, 60 and 100 ms; spray distance $z = 20$ mm.

let us focus on $\Delta t = 60$ ms. In this example, h increases rapidly to 15 kW m^{-2} K^{-1} within 5 ms. During the rest of the spurt duration, $h(t)$ fluctuates around an average value of 18 kW m^{-2} K^{-1}, until the spurt terminates. Then, $h(t)$ increases further to 22 kW m^{-2} K^{-1} and remains at this value for 20 ms. It then drops to 19 to 17 kW m^{-2} K^{-1} before starting to diminish rapidly at 120 ms. The dynamic variations of $h(t)$ are similar for different Δt. All show a higher average $h(t)$ after a short period of rapid increase, followed by an even higher average $h(t)$ after spurt termination. This behaviour suggests the presence of a very thin liquid layer which evaporates more efficiently upon spurt termination, which is why h oscillates around a relatively constant value. The existence of this layer, however, is not as noticeable as that resulting from spurts delivered at $z = 50$ mm, and it is clearly

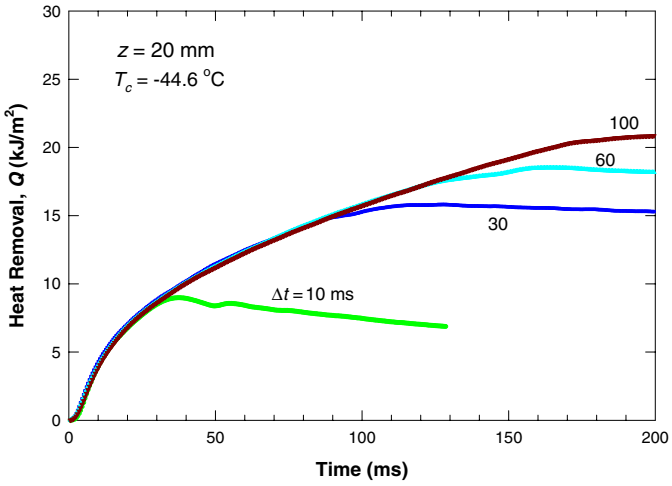

Figure 9. Estimated total heat removal per unit area (Q) as a function of time for spurt durations: $\Delta t = 10$, 30, 60 and 100 ms; spray distance $z = 20$ mm.

more unstable as evidenced by the large fluctuations seen in figure 8. Also, note that for very high values of $h(t)$, the cooling time after spurt termination becomes relatively shorter as Δt increases. For example, the cooling time lasts about 90 ms for a 30 ms spurt, 120 ms for a 60 ms spurt and only 175 ms for a 100 ms spurt.

The corresponding total heat removal, Q is given in figure 9. Note that at any given time, higher values of Q are obtained for spurts at $z = 20$ mm than for those at $z = 50$ mm (figure 5). For example, for $z = 20$ mm, a $\Delta t = 30$ ms leads to $Q \sim 15.2$ kJ m^{-2} at 100 ms, whereas for $z = 50$ mm, the same spurt duration leads to $Q \sim$ 12–13 kJ m^{-2} ($\sim$20% difference), also at 100 ms.

4. Discussion on heat transfer mechanisms during CSC

The surface heat transfer mechanisms during CSC may be better understood if q is plotted as a function of surface temperature. Figure 10 shows two curves corresponding to $z = 50$ and 20 mm, both for the same Δt of 40 ms. Classical boiling theory can be employed to explain the variation in q with surface temperature. At the beginning of the spurt, when the surface temperature is high, heat transfer between the surface and the impinging cryogen droplets occurs within the transition boiling regime, where as the droplets impinge onto the surface, a layer of vapour is formed between the surface and liquid cryogen layer. However, the surface temperature is always below the Leidenfrost temperature, which is a distinct characteristic of the boiling process of liquids. At the Leidenfrost temperature, q shows a local minimum when plotted as a function of the superheat (i.e., the temperature difference between the surface and the liquid's boiling temperature). This indicates the presence of a vapour layer, which disrupts the heat transfer across the surface, resulting in lower values of q. As the surface temperature further decreases below the Leidenfrost temperature, q increases as more efficient surface wetting and boiling occur, leading to an even larger q. Eventually, the entire surface becomes available for wetting and the surface heat flux reaches a maximum q_c (also called critical heat flux). As the surface temperature is further reduced, the heat transfer process moves into the nucleate boiling

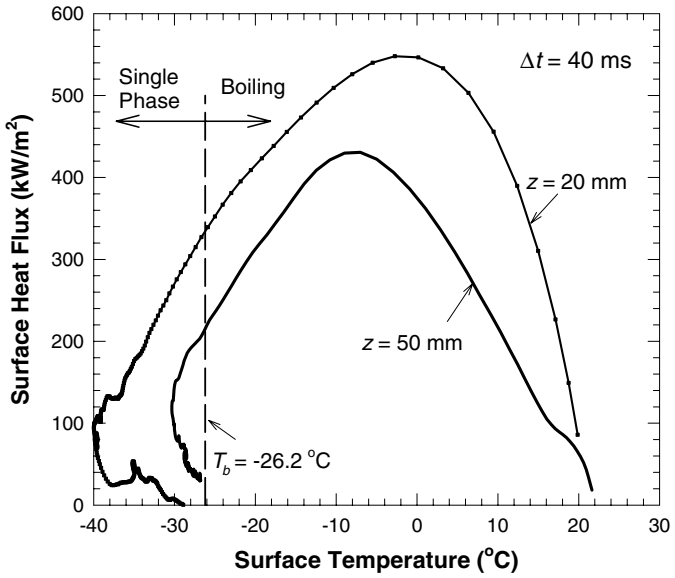

Figure 10. Estimated surface heat flux, q, as a function of surface temperature for spurt duration $\Delta t = 40$ ms and spray distances $z = 50$ and 20 mm, respectively.

regime, where q is proportional to the amount of bubbles nucleated on the surface. As the surface temperature further decreases, the surface superheat also decreases, leading to less bubble nucleation and, therefore, a lower q. Finally, when the surface temperature is reduced to a minimum superheat level, nucleate boiling stops and single-phase heat transfer takes place between the surface and the liquid, leading to a very low q. Both of these boiling curves are qualitatively similar to those observed for a water spray when the surface temperature is below the Leidenfrost temperature (see, e.g., Ciofalo *et al* (1999) and Bernardin *et al* (1997)).

Figure 10 also shows the marked effect of z on $q(t)$. Shortening z from 50 to 20 mm not only increases significantly q_c from 431 to 548 kW m^{-2}, but it also broadens the region with high q. The surface temperature at which q_c occurs also becomes higher, being about -1.1 °C for $z = 20$ mm versus -7.7 °C for $z = 50$ mm. The higher $q(t)$ for $z = 20$ mm is due to a strong interaction between cryogen droplets and the surface. As indicated in our previous paper (Aguilar *et al* 2003), the spray–surface interactions for short z (<25 mm) are very different from those of longer z (>25 mm). In the case of longer spray distances, the cryogen reaches the surface finely atomized and the droplets are smaller and colder due to continuous in-flight evaporation. For a shorter z, the sprays show jet-like characteristics, containing larger and faster cryogen droplets (Aguilar *et al* 2000) that reach the surface more forcefully and, therefore, can penetrate deeper into the liquid layer, allowing cold droplets to make direct contact with the surface throughout most of the spurt duration. In addition, the impingement of large droplets also mixes more thoroughly the liquid layer, improving the heat removed by single-phase convection. The combination of these events results in a higher q. This forceful impact also leads to rebound and splashing of the cryogen droplets during the spurt. As a result, less cryogen remains on the surface during and after the spurt and, thus, a shorter cooling time results (Aguilar *et al* 2003).

It is obvious that clinical conditions are different from those used for the laboratory experiments presented herein. First, normal human skin temperature is about 30–31 °C, whereas the skin-like thermal substrate had an initial temperature of ∼20 °C. The higher skin temperature (1.5 times) would lead to a higher superheat, which in turn would enhance q. Secondly, laser light absorbed by the epidermis, which is not resembled in our experiments, provides an additional heat source that would also enhance q. In contrast to these two effects, the lower thermal diffusivity of skin compared to that of the thermal substrate (∼2.7 times) would lead to lower q on skin. The latter effect may actually cancel out or at least mitigate the differences between the experimental and clinical conditions.

From a clinical standpoint, it may be deduced that, for the spray distances and skin phantom model studied, further prolonging Δt beyond 40 ms will only increase the thickness of the liquid cryogen layer and will not further reduce the surface temperature, which means that longer spurts will have a negligible impact on both q and Q. One should keep in mind, however, that longer Δt lead to the formation of a thicker cryogen layer, which may remain on the skin surface long after laser heating. As this layer evaporates it could remove epidermal heat immediately following laser heating and, therefore, reduce the risk of epidermal damage. This is indeed in agreement with the recent work by Tunnell *et al* (2000), who showed that spurts longer than 40 ms decrease the amount of epidermal thermal damage.

5. Summary and conclusions

Experiments have been performed to investigate the heat transfer dynamics during CSC using a fast-response temperature sensor. An IHCP algorithm is used to estimate q and h as functions of time.

q reveals a marked dynamic variation during CSC with a maximum heat flux (q_c) occurring during the early stages of the spurt, followed by a quick decrease. The presence of q_c during CSC can be understood through classic boiling theory as a transition from transition to nucleate boiling. As the surface temperature drops close to the cryogen boiling temperature (−26 °C), heat transfer is dominated by surface evaporation, which lasts until the entire cryogen layer evaporates. The latter process may persist long after spurt termination.

For a long spray distance ($z = 50$ mm), the cooling rate is much lower than that of $z = 20$ mm. The estimated q_c vary from 450 to 600 kW m^{-2} for $z = 50$ and 20 mm, respectively, corresponding to h maxima values of 10 kW m^{-2} K^{-1} and 17–22 kW m^{-2} K^{-1}.

For $z = 50$ mm, spurts longer than 40 ms do not increase the total heat removal (Q) within the first 200 ms. For $z = 20$ mm, however, spurt durations (Δt) longer than 100 ms are required to achieve the same Q.

Based on the skin phantom studied, Δt longer than 40 ms will have a negligible impact on both q and Q from skin within the cooling time range used by most clinical applications (10–100 ms).

Acknowledgments

This work was supported by the National Institutes of Health (GM 62177 and AR 47551 to JSN and HD42057 to GA). Institutional support from the Beckman Laser Institute Endowment is also acknowledged. Laboratory assistance and data analysis provided by Emil Karapetian, Odette Ma and Misha Heller are greatly appreciated.

References

Aguilar G, Diaz S H, Lavernia E J and Nelson J S 2002 Cryogen spray cooling efficiency: improvement of port wine stain laser therapy through multiple-intermittent cryogen spurts and laser pulses *Lasers Surg. Med.* **31** 27–35

Aguilar G, Majaron B, Pope K, Svaasand L O, Lavernia E J and Nelson J S 2001a Influence of nozzle-to-skin distance in cryogen spray cooling for dermatologic laser surgery *Lasers Surg. Med.* **28** 113–20

Aguilar G, Majaron B, Verkruysse W, Nelson J S and Lavernia E J 2000 Characterization of cryogenic spray nozzles with application to skin cooling *Proc. Int. Mechanical Engineering Congress and Exposition (IMECE) (Orlando, FL)* vol 253 pp 189–97

Aguilar G, Majaron B, Verkruysse W, Zhou Y, Nelson J S and Lavernia E J 2001b Theoretical and experimental analysis of droplet diameter, temperature, and evaporation rate evolution in cryogenic sprays *Int. J. Heat Mass Transfer* **44** 3201–11

Aguilar G, Verkruysse W, Majaron B, Svaasand L O, Lavernia E J and Nelson J S 2001c Measurement of heat flux and heat transfer coefficient during continuous cryogen spray cooling for laser dermatologic surgery *IEEE J. Sel. Top. Quantum Electron.* **7** 1013–21

Aguilar G, Wang G-X and Nelson J S 2003 Dynamic cooling behavior during cryogen spray cooling: effects of spurt duration and spray distance *Lasers Surg. Med.* **32** 152–9

Anvari B, Milner T E, Tanenbaum B S and Nelson J S 1998 A comparative study of human skin thermal response to sapphire contact and cryogen spray cooling *IEEE Trans. Biomed. Eng.* **45** 934–41

Beck J V, Blackwell B and St Clair C R 1985 *Inverse Heat Conduction: Ill-Posed Problems* (New York: Wiley)

Bernardin J, Stebbins C J and Mudawar I 1997 Mapping of impact and heat transfer regimes of water drops impinging on a polished surface *Int. J. Heat Mass Transfer* **40** 247–67

Chang C J, Anvari B and Nelson J S 1998 Cryogen spray cooling for spatially selective photocoagulation of hemangiomas: a new methodology with preliminary clinical reports *Plast. Reconstr. Surg.* **102** 459–63

Ciofalo M, Di Piazza I and Brucato V 1999 Investigation of the cooling of hot walls by liquid water sprays *Int. J. Heat Mass Transfer* **42** 1157–75

Duck F A 1990 Thermal properties of tissue *Physical Properties of Tissue* (London: Academic)

Kelly K M, Nelson J S, Lask G P, Geronemus R G and Bernstein L J 1999 Cryogen spray cooling in combination with non-ablative laser treatment of facial rhytides *Arch. Dermatol.* **135** 691–4

Majaron B, Verkruysse W, Kelly K M and Nelson J S 2001 Er:YAG laser skin resurfacing using repetitive long-pulse exposure and cryogen spray cooling: II. Theoretical analysis *Lasers Surg. Med.* **28** 469–76

Nelson J S, Majaron B and Kelly K M 2000 Active skin cooling in conjunction with laser dermatologic surgery: methodology and clinical results *Semin. Cutan. Med. Surg.* **19** 253–66

Nelson J S, Milner T E, Anvari B, Tanenbaum B S, Kimel S, Svaasand L O and Jacques S L 1995 Dynamic epidermal cooling during pulsed laser treatment of port-wine stain *Arch. Dermatol.* **131** 695–700

Pfefer T J, Smithies D J, Milner T E, van Gemert M J C, Nelson J S and Welch A J 2000 Bioheat transfer analysis of cryogen spray cooling during laser treatment of port wine stains *Lasers Surg. Med.* **26** 145–57

Svaasand L O, Randeberg L L, Aguilar G, Majaron B, Kimel S, Lavernia E J and Nelson J S 2003 Cooling efficiency of cryogen spray during laser therapy of skin *Lasers Surg. Med.* **32** 137–42

Taler J 1996 Theory of transient experimental techniques for surface heat transfer *Int. J. Heat Mass Transfer* **39** 3733–48

Torres J H, Tunnell J W, Pikkula B and Anvari B 2001 An analysis of heat removal during cryogen spray cooling and effects of simultaneous airflow application *Lasers Surg. Med.* **28** 477–86

Tunnell J W, Nelson J S, Torres J H and Anvari B 2000 Epidermal protection with cryogen spray cooling during high fluence pulsed dye laser irradiation: an *ex vivo* study *Lasers Surg. Med.* **27** 373–83

Tunnell J W, Torres J H and Anvari B 2002 Methodology for estimation of time-dependent surface heat flux due to cryogen spray cooling *Ann. Biomed. Eng.* **30** 19–33

Verkruysse W, Majaron B, Tanenbaum B S and Nelson J S 2000 Optimal cryogen spray cooling parameters for pulsed laser treatment of port wine stains *Lasers Surg. Med.* **27** 165–70

Waldorf H A, Alster T S, McMillan K, Kauvar A N, Geronemus R G and Nelson J S 1997 Effect of dynamic cooling on 585-nm pulsed dye laser treatment of port-wine stain birthmarks *Dermatol. Surg.* **23** 657–62